Pergamon

Int. J. Heat Mass Transfer. Vol. 39, No. 11, pp. 2205–2219, 1996

0017-9310/96 $15.00 + 0.00

0017-9310(95)00324-X

A numerical study of droplet–vortex interactions in an evaporating spray

T. W. PARK† and S. K. AGGARWAL‡
Department of Mechanical Engineering, University of Illinois at Chicago, Chicago, IL 60607, U.S.A.

and

V. R. KATTA§
System Research Laboratory, Inc., Dayton, OH 45440, U.S.A.

(*Received* 23 *March* 1995 *and in final form* 28 *August* 1995)

Abstract—In this paper, we present the time-dependent axisymmetric numerical simulation of a n-heptane evaporating spray, and investigate the droplet–vortex interactions which determine the structural and dynamic characteristics of a spray jet flow. The spray is formed between a droplet-laden heated nitrogen jet and a coflowing air stream. A detailed, multidimensional, two-phase algorithm is developed for the simulation. Monodisperse spray is introduced into the large vortex structures that are generated by the buoyancy-induced hydrodynamic instability of the heated jet. Results focus on the two-way interactions between vortical structures and droplets, and the dynamics of both non-evaporating and evaporating sprays. The vortex structures cause droplets to disperse radially outward, and this in turn determines the fuel vapor distribution and also modifies the vortex dynamics. Thus, the dynamics and structural characteristics of evaporating sprays are strongly influenced by the two-way transient interactions. The effects of initial droplet size, injection location, and liquid-to-gas mass loading ratio on these interactions are investigated. These studies indicate that the effect of dispersed phase on gas phase is negligible for mass loading ratio less than 0.5. At higher mass loading ratios, the dispersed phase modifies the dynamics of vortex structures but not the time-average behavior for non-evaporating spray, while for evaporating spray it influences both the dynamics and the time-averaged behavior. It is also found that the spray injection characteristics have strong influence on the processes of droplet–vortex interactions. Copyright © 1996 Elsevier Science Ltd.

INTRODUCTION

Large-scale, coherent vortical structures have been found to exist in a variety of shear flows including those involving combustion and multiple phases [1–4]. In two-phase shear flows involving solid particles or liquid droplets, the transient interactions between dispersed phase and large vortical structures are expected to play a central role in determining the dynamics and structural characteristics of these flows. The transient interactions pertain to the effect of large vortical structures on the behavior of droplets/particles, and the influence of droplets on the dynamics of large vortical structures. These two effects coupled in a nonlinear manner; the vortex structures determine the droplet dispersion and gasification behavior, which in turn affects the local environment surrounding each droplet and thereby the dynamics of the two-phase system under consideration. Several numerical [5, 6] and experimental [7–10] studies in recent years have focused on the one-way coupling, examining the influence of large eddies on the dynamics of droplets/particles injected into a shear flow. These studies show that the effect of large structures on particle motion is characterized by the ratio of particle response time to characteristic time of structures. This ratio is defined as the Stokes number (St). When the particle response time is of the same order of magnitude as the vortex time scale, $St \sim O(1)$, particles can disperse significantly more than the fluid particles, the enhanced dispersion being attributed to the centrifugal action of vortices. For small Stokes number, $St \ll 1.0$, particles behave similar to the fluid particles, while for large Stokes number, particles remain largely unaffected by the vortices. More recent works [11, 12] on particle-laden flows have examined the effect of external forcing on the particle dispersion behavior. A general observation from these studies [11, 12] is that the dynamics of vortex structures, and thereby the dispersion behavior of particles in a shear layer can be manipulated by a subharmonic forcing of the shear layer.

Particle-laden shear flows in practical applications

† Currently at Wright Laboratory, Aero Propulsion and Power Directorate, Wright-Patterson Air Force Base, OH 45433, U.S.A., as a National Research Council Research Associate.

‡ Author to whom correspondence should be addressed.

§ Present address: Innovative Scientific Solutions, Inc., Dayton, OH 45430, U.S.A.

NOMENCLATURE

C_p	specific heat
d_o	initial droplet diameter
D	vapor/air binary diffusion coefficient
g	acceleration of gravity
h_{fs}	enthalpy of fuel vapor at droplet surface
$l_{k,eff}$	effective latent heat, or the heat transferred from gas phase to droplet
$\dot{m}_k$	droplet vaporization rate
M	ratio of the liquid fuel mass flow rate to the nitrogen mass flow rate
M_k	mass of each group of droplets
n_k	number of droplets in each group
p	pressure
r	radial distance
t	time
T	temperature
u	axial velocity
v	radial velocity
Y	mass fraction
z	axial distance.

Greek symbols

μ	dynamic viscosity
λ	thermal conductivity
ρ	density.

Subscripts

f	fuel vapor
g	gas-phase
k	droplet characteristic
l	liquid-phase
o	oxygen
s	surface.

involve two-way, nonlinear interactions between the continuous and dispersed phases. Previous studies cited above focus mainly on the one-way interactions, i.e. on characterizing the effect of vortex structures on droplet motion and dispersion behavior. The effects of dispersed phase on vortex dynamics, and subsequently on fuel vapor distribution and flame behavior remain largely unexplored. In this paper, we report a numerical study of two-way droplet–vortex interactions in an unsteady evaporating spray. The spray is formed between a droplet-laden heated nitrogen jet and a coflowing air stream. The jet velocity and temperature are considered in a range where the large vortical structures are generated due to the buoyancy-induced hydrodynamic instability rather than the shear-induced Kelvin–Helmholtz instability. The vaporization characteristics of n-heptane fuel spray under the influence of two-way droplet–vortex interactions are investigated. The additional complexities due to chemical reactions and heat release are avoided so as to focus on the dynamics of two-way interactions. A non-evaporating spray is also analyzed in order to distinguish the interactions involving only momentum transfer between the phases from those involving mass, momentum, and energy transfer. Results are presented that highlight the dynamics as well as the time-averaged structure of these sprays.

PHYSICAL MODEL

The evaporating spray investigated in the present study is shown schematically in Fig. 1. It consists of a central fuel jet which is a two-phase mixture of gaseous nitrogen and liquid fuel droplets and a low-speed coannulus air flow. The central jet is heated primarily to enhance the fuel evaporation; however, in the present studies, it also plays a key role for the formation of buoyancy induced vortical structures. Numerical studies on the two-way interactions between the vor-

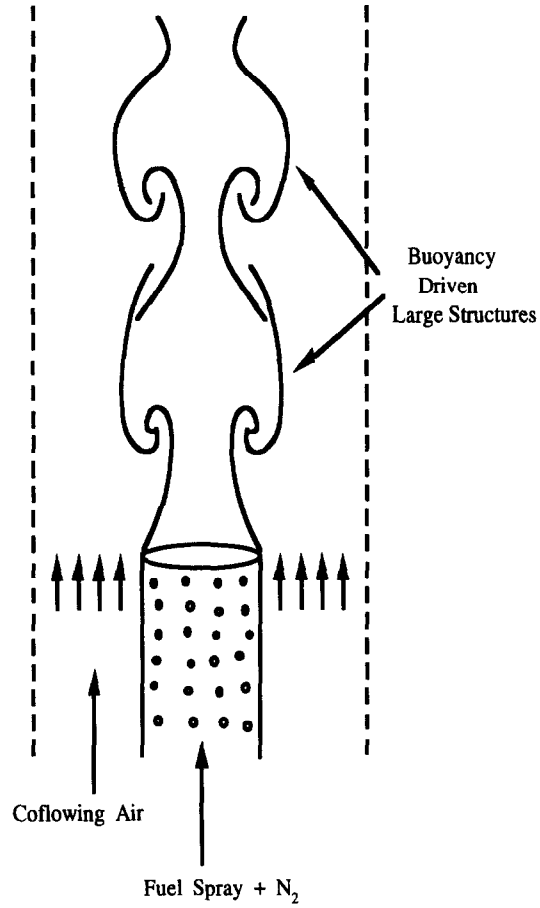

Fig. 1. A schematic of evaporating spray jet at 1 g.

Table 1. Transport coefficients and source terms appearing in governing equations

Equations	Φ	Γ^{Φ}	S_g^{Φ}	S_l^{Φ}
Continuity	1	0	0	$\sum_k n_k \dot{m}_k$
Axial momentum	u	μ	$-\frac{\partial p}{\partial z}+(\rho_o-\rho)g+\frac{\partial}{\partial z}\left(\mu\frac{\partial u}{\partial z}\right)+\frac{\partial}{\partial r}\left(\mu\frac{\partial v}{\partial z}\right)+\frac{\mu}{r}\frac{\partial v}{\partial z}$ $-\frac{2}{3}\left\{\frac{\partial}{\partial z}\left(\mu\frac{\partial u}{\partial z}\right)+\frac{\partial}{\partial z}\left(\mu\frac{\partial v}{\partial r}\right)+\frac{\partial}{\partial z}\left(\mu\frac{v}{r}\right)\right\}$	$\sum_k\left(n_k\dot{m}_k u_k-n_k M_k\frac{du_k}{dt}\right)$
Radial momentum	v	μ	$-\frac{\partial p}{\partial r}+\frac{\partial}{\partial z}\left(\mu\frac{\partial u}{\partial r}\right)+\frac{\partial}{\partial r}\left(\mu\frac{\partial v}{\partial r}\right)+\frac{\mu}{r}\frac{\partial v}{\partial r}-2\mu\frac{v}{r^2}$ $-\frac{2}{3}\left\{\frac{\partial}{\partial r}\left(\mu\frac{\partial u}{\partial z}\right)+\frac{\partial}{\partial r}\left(\mu\frac{\partial v}{\partial r}\right)+\frac{\partial}{\partial r}\left(\mu\frac{v}{r}\right)\right\}$	$\sum_k\left(n_k\dot{m}_k v_k-n_k M_k\frac{dv_k}{dt}\right)$
Mass fraction of fuel	Y_f	ρD_f	0	$\sum_k n_k \dot{m}_k$
Mass fraction of oxygen	Y_o	ρD_o	0	0
Energy	T	λ/C_p	0	$\sum_k n_k \dot{m}_k (h_{fs}-l_{k,eff})$

tex structures and the evaporating droplets are conducted by solving the unsteady, axisymmetric gas-phase equations that include the droplet source terms, and the appropriate droplet equations.

The unsteady, axisymmetric governing equations in cylindrical (z, r) coordinate system for a droplet-laden heated jet are

$$\frac{\partial(\rho\Phi)}{\partial t}+\frac{\partial(\rho u\Phi)}{\partial z}+\frac{\partial(\rho v\Phi)}{\partial r}=\frac{\partial}{\partial z}\left(\Gamma^{\Phi}\frac{\partial\Phi}{\partial z}\right)+\frac{\partial}{\partial r}\left(\Gamma^{\Phi}\frac{\partial\Phi}{\partial r}\right)-\frac{\rho v\Phi}{r}+\frac{\Gamma^{\Phi}}{r}\frac{\partial\Phi}{\partial r}+S_g^{\Phi}+S_l^{\Phi}. \quad (1)$$

The general form of equation (1) represents the continuity, momentum, species, or energy conservation equation depending on the variable used for Φ. Table 1 gives the transport coefficients Γ^{Φ} and the source terms S_g^{Φ} and S_l^{Φ} that appear in the governing equations. In this table, μ, λ and C_p represent the viscosity, the thermal conductivity and the specific heat, respectively. They are considered functions of temperature and species concentration.

The effect of dispersed phase on gas-phase properties is incorporated through the source/sink terms (S_l^{Φ}), representing the exchange of mass, momentum, and energy between the gas and liquid phases. In order to evaluate these terms, it is necessary to establish droplet trajectories, size and temperature histories. The Lagrangian approach is employed to solve the liquid-phase governing equations for the dynamics and vaporization history of each droplet group. The spray is characterized by a discrete number of droplet groups, distinguished by their injection location, initial size and time of injection. A droplet group in a Lagrangian treatment represents a characteristic containing a finite number of droplets. Since an axisymmetric configuration is analyzed, the liquid properties are implicitly averaged in the azimuthal direction and the number of droplets associated with each characteristic represents droplets uniformly distributed in an annual ring. The equations governing the variation of position, velocity, and size for each droplet group and other expressions are available in ref. [13]. A comprehensive vaporization model is employed to calculate the instantaneous droplet size and surface temperature along the trajectory of each group. The model includes the effects of variable thermophysical properties, non-unity Lewis number in the gas film outside the droplet, the effect of Stefan flow on the heat and mass transfer between the droplet and the gas, and the effect of transient liquid heating. The variable thermophysical properties are calculated at reference film temperature and concentrations, obtained by using the 1/3 rule, except for the gas density which is calculated at the free stream value [14]. The Wilke rule [15] is used to calculate the dynamic viscosity and thermal conductivity of the gas film. The liquid fuel (n-C_7H_{16}) properties are collected from the various sources and approximated as a function of the temperature [13]. The effect of transient liquid heating is incorporated by using the finite-conductivity model [16]. This model is deemed satisfactory in the present study, since the maximum droplet Reynolds number during droplet lifetime is less than ten and thus the effect of internal circulation is expected to be negligible. For the same reason, the effects of gas-phase convection on the heat and mass transport are represented by the Ranz–Marshall correlation [16].

SOLUTION PROCEDURE

The numerical solution of the unsteady two-phase equations employs an implicit algorithm for solving the gas-phase equations, and an explicit Runge–Kutta procedure for the liquid-phase equations. The finite-

difference forms of the momentum equations are obtained using an implicit QUICKEST scheme [17], while those of the species and energy equations are obtained using a hybrid scheme of Spalding [18]. A "finite control volume" approach with a staggered, non-uniform grid system is utilized. Body force term due to gravitational field is included in the axial momentum equation for gas-phase and the droplet motion equation for liquid-phase. An iterative ADI (Alternative Direction Implicit) technique is used for solving the resulting sets of algebraic equations. A stable numerical integration procedure is achieved by coupling the species and energy equations through the source terms (cf. Table 1). At every time step, the pressure field is calculated by solving the pressure Poisson equations simultaneously and utilizing the LU (Lower and Upper diagonal) matrix decomposition technique. It should be noted that the pressure Poisson equations consider the effect of mass transfer from the liquid phase to the gas phase, represented by a source term in the gas-phase mass continuity equation.

The liquid-phase equations are advanced in time by a second-order accurate Runge–Kutta method. Since the gas-phase solution employs an implicit procedure, the temporal step size used for integrating the liquid-phase equations is smaller than that for gas-phase equations. An automatic procedure is implemented in order to select an optimum liquid-phase time step. The procedure involves calculating the characteristic thermal response time, velocity response time and vaporization time for each droplet group, and then selecting the temporal step size as a fraction (one-hundredth) of the smallest of these time scales. A detailed examination of the various time scales, based on numerical experiments, revealed that the temporal step size is determined by either the thermal response time or the velocity response time of a given droplet group. The number of subcycles for advancing the liquid-phase solution for each gas-phase cycle typically varies from two to ten, depending upon the droplet size.

The procedure to advance the two-phase solution over one gas-phase time step is as follows. Using the known gas-phase properties, the liquid-phase equations are solved over a specified number of liquid-phase subcycles. A third-order accurate Lagrangian polynomial method is used for interpolating the gas-phase properties from the non-uniform fixed grid to the droplet characteristic location. It should be noted that the interpolation scheme for the gas-phase velocities u and v is based on their respective grid cells because of the use of a staggered grid in gas-phase calculation. The droplet properties are updated after every liquid-phase subcycle. Also, during each subcycle, the liquid-phase source terms appearing in the gas-phase equations are calculated at the characteristic location, and then distributed to the surrounding gas-phase grid points. These source terms are added at each gas-phase grid points during one gas-phase time step and then used in the implicit solution of the gas-phase equations.

RESULTS

The jet diameter of the vertically mounted evaporating spray considered in the present study is 2.54 cm. The jet velocities for the central fuel and coannular air streams are 1.0 and 0.2 m s^{-1}, respectively. Flat velocity profiles are used as the inflow conditions. Temperature chosen for the fuel jet is 1200 K while that of the surrounding annulus air is 294 K. Calculations are made for a physical domain having dimensions of 15 and 40 cm in the radial and axial direction, respectively. It should be noted that the physical domain used in the calculations is much larger than the domain of interest (3×20 cm) and hence, the results are not influenced by the computational boundaries. Results reported in the present paper are obtained using a grid system having 151 and 61 points in the axial and radial directions, respectively. Grid lines are clustered near the shear layer to resolve the steep gradients of the dependent variables. Calculations are advanced in time utilizing a low CFL number of 0.2. In an earlier study [13], it was found that the results obtained on a 151×61 mesh system (with grid spacings similar to the ones used in the present investigation) and using a CFL number less than 0.5 are grid independent and time accurate.

Numerical experiments are conducted by injecting different groups of droplets into the fuel stream to examine the changes in the flow structure due to the two-way nonlinear, two-phase interactions. The injection process consists of introducing a group of monodisperse droplets at a given instant of time. The number of droplets in each group depends on the mass loading (ratio of the liquid fuel mass flow rate to the nitrogen mass flow rate), initial droplet size, and injection time interval. As a base case for the spray calculations reported in this work, a monodisperse n-heptane spray with an initial diameter of 200 μm and mass loading of unity is considered. At a mass loading of unity, the volume occupied by liquid phase is about three orders of magnitude smaller than that of the gas-phase volume due to the high density of the liquid fuel and hence, the dilute-spray assumption is still valid. At higher mass loading, however, the assumption would become increasingly more questionable. For this reason, the mass loading of unity is the highest loading considered in the present study. The droplets are injected continuously into the jet shear layer from a radial location of 1.25 cm. A time difference of 1.428 ms ($=9\,\Delta t_{\text{gas}}$) is used between two consecutive injections for all the spray calculations reported in this work. This time interval was determined based on the constraint that the spatial separation between two successive droplet groups is large enough for neglecting the interaction between the droplets. This yields the number of droplets in each group to be 76. Three different droplet injection intervals are chosen to examine their effect on the time-averaged temperature and axial velocity profiles in the flow field. Figure 2 shows the time-averaged axial profiles of

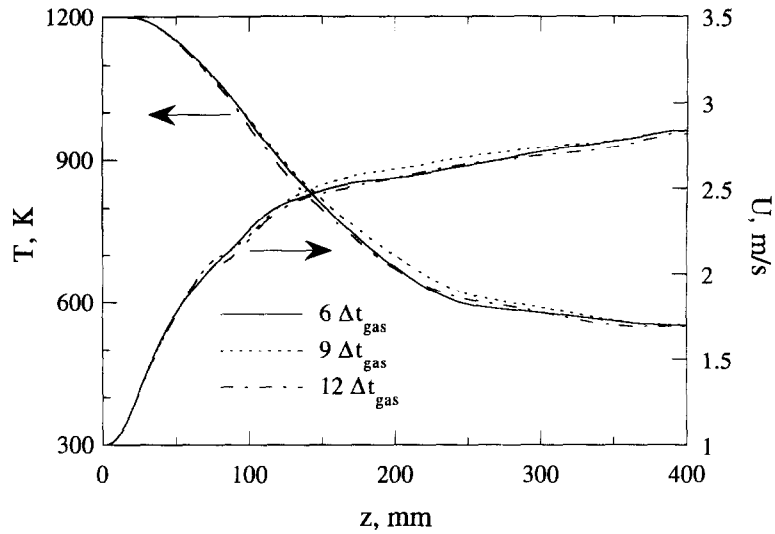

Fig. 2. Effect of droplet interval on the time-averaged temperature and axial velocity profiles of 200-μm evaporating spray with mass loading value of $M = 1.0$.

temperature and axial velocity for the three cases. As expected, the average temperature decreases along the jet axis due to gas-phase heat transport processes and cooling caused by the dispersed phase. The average axial velocity, however, increases in the axial direction due to buoyant acceleration. The important observation is that the gas-phase calculations are not sensitive to the droplet injection interval used for the base case.

The effect of dispersed phase on the dynamics of vortex structures and heated jet is portrayed in Figs. 3 and 4. Calculations are initially made without injecting droplets into the fuel stream. The shear layer between the 1200-K nitrogen jet and the cold annulus air flow became unsteady with the development of large-scale vortices. Iso-temperature contours of this heated jet are shown in Fig. 3(a). It is important to note that these vortical structures are generated without using any external forcing, and their dynamics is found to be highly periodic. The role of gravity on the

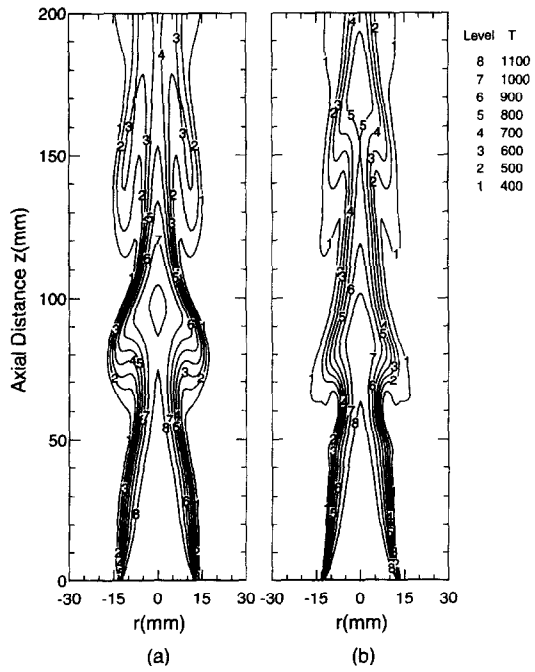

Fig. 3. Instantaneous iso-temperature contours for the heated jet: (a) without fuel spray; (b) with fuel spray.

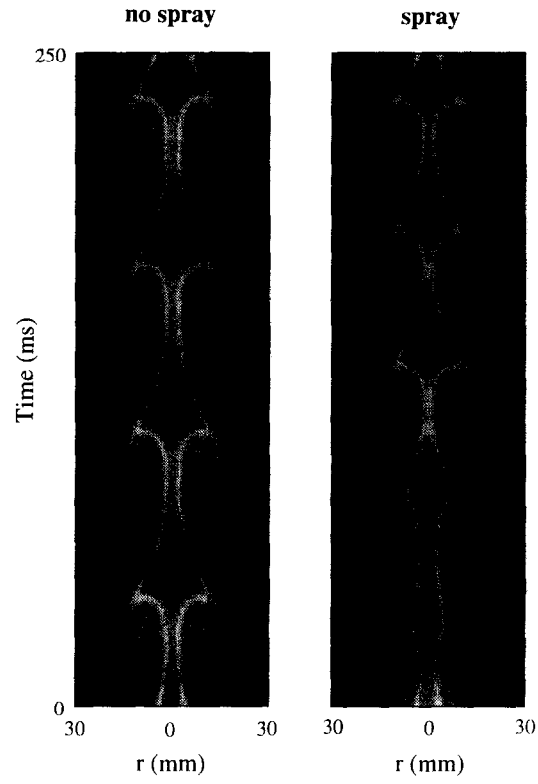

Fig. 4. Time evolution of temperature contours at axial location of 10 cm above the inlet for the cases of Fig. 3.

dynamics of the heated jet was confirmed by performing numerical experiments. When the gravitational term in the axial momentum was set equal to zero, the simulation yielded a steady laminar jet flow. This observation is in contrast with that made for heated jet flows at higher Reynolds number, in which Kelvin–Helmholtz instabilities develop independent of the assumption made for gravitational force. Most of the experimental studies on heated jets [19, 20] were focused on the higher Reynolds-number flow and did not provide insight on buoyancy-induced instabilities. However, the latter ones were extensively investigated experimentally in jet diffusion flames [21, 22] and helium jets [23]. The numerical studies [24, 25] performed on these flames and helium jet flows using the code discussed in the present study predicted the growth of buoyancy-induced instabilities very accurately.

Instantaneous iso-temperature contours for the case with fuel spray [plotted in Fig. 3(b)] are compared with the ones obtained without introducing fuel spray in Fig. 3(a). All the droplet source terms (Table 1) are incorporated in the gas-phase equations for the simulation with fuel spray. For both the cases, the buoyancy-induced vortex structures shown in Fig. 3 appear naturally without any external forcing. It is apparent from the figure that the injection of 200-μm droplets into the shear layer weakened the vortical structures and decreased the spreading of the heated jet. The weakening of vortical structures is probably caused by the cooling effect of the dispersed plane, while the decrease in the spreading rate may be expected due to fact that the addition of fuel spray to the nitrogen gas increases the jet momentum. Figure 3 further indicates that the jet oscillations are highly coherent for the gaseous (no spray) case and somewhat less coherent for the spray case. Since the presence of liquid phase modifies the spectral characteristics or the dominant instability frequency, an attempt was made to phase-lock the instantaneous images for the two cases. Consequently, the temperature contour plots in Fig. 3 for the gaseous and spray cases represent the results that are obtained at slightly different times from the start of the respective calculation.

The dynamics of vortex structures is examined by plotting the time evolution of temperature contours in Fig. 4. Temperature data along the radial location at an axial location of 10 cm above the jet exit for the gaseous and spray cases are recorded over a time period of 250 ms and shown in this figure. Again, an attempt was made to phase-lock the images for the gaseous and spray case. It can be seen from Fig. 4(a) that the vortex structures in the case of gaseous jet are highly coherent and periodic. With the addition of fuel spray the dynamics of jet has become aperiodic and the vortex crossing frequency (obtained by counting the number of vortices in a fixed time interval) has increased by about 30%. This can be confirmed by performing the spectral analysis at different axial locations in the shear layer. Temperature data were recorded at different locations during more than 10 vortex crossing times (4096 Δt_{gas}). Figure 5 clearly shows that the dominant frequency for the spray case is increased to 20.5 Hz which is about 30% higher compared to the frequency observed for the gaseous jet case. In addition, the deterioration in coherency can be seen for the spray case. The increase in frequency for the spray case is resulting from the momentum transfer between the liquid drops and the gaseous flow. The fuel drops are injected into the gaseous jet shear layer at the same velocity as that of the local gas velocity which yields higher momentum to the fuel drops. As the gaseous flow and drops convect downstream, the higher momentum of the latter transfer to the former which, in turn, increases the local gas velocity. As a result, the crossing frequency of the vortices in the shear layer, which is proportional to the local gas velocity, also increases. The increase in frequency is observed for both non-evaporating and evaporating sprays, implying again that this is primarily a momentum-transfer effect. It is also interesting to note that no vortex merging is observed for these two cases.

Effect of liquid mass loading

The structural changes noted in a buoyancy driven heated jet with the addition of fuel spray are resulting from (1) liquid mass loading, (2) droplet evaporation and (3) the two-way interaction between vortices and droplets. To further understand the impact of the above individual parameters, numerical experiments are performed by changing the liquid mass loading, evaporation characteristics, spray injection location and droplet size.

The instantaneous iso-temperature contours for five different mass loading values ($M = 0$, 0.125, 0.25, 0.5 and 1.0) for a non-evaporating spray are shown in Fig. 6. Again, the images shown in Fig. 6 are phase locked. Liquid mass flow rate is controlled by changing the number of droplets in each injected group. As the droplets are assumed to be non-evaporating in this case, only the source terms in the momentum equation (cf. Table 1) are considered in the gas-phase equations. In other words, only the momenta are exchanged in this two-phase flow calculation. The single-phase gaseous flow shown in Fig. 3(a) may be approximated as a non-evaporating spray in the limiting case of $M = 0$ [Fig. 6(a)]. It seems that the structural characteristics of low mass loading cases like $M = 0.125$ and 0.25 are similar to that of single-phase flow even though the vortex-crossing frequencies in these flows are somewhat different. The time history plots of the dynamic heated jets for different mass loading values are shown in Fig. 7. This plot clearly shows the changes in the sizes of the vortex structures and their crossing frequency for different cases. It may be observed from Fig. 7 that as the mass loading ratio is increased, the crossing frequency of vortex structures is also increasing. At higher mass loading

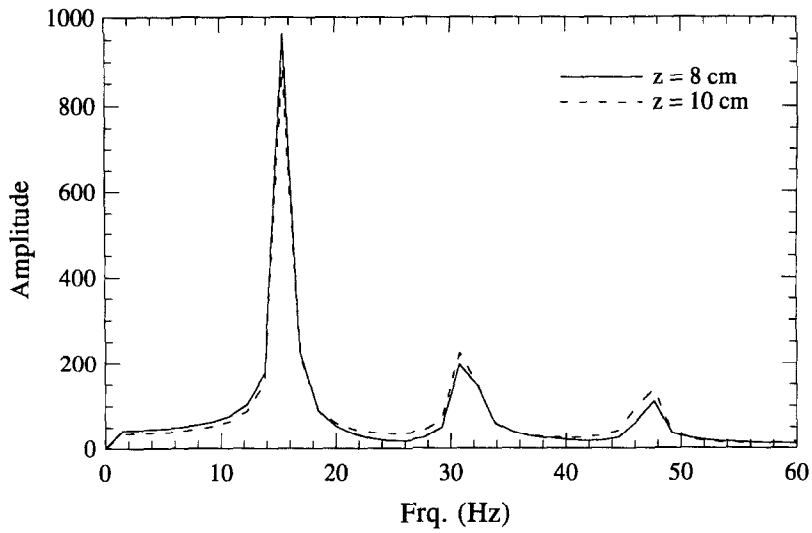

(a)

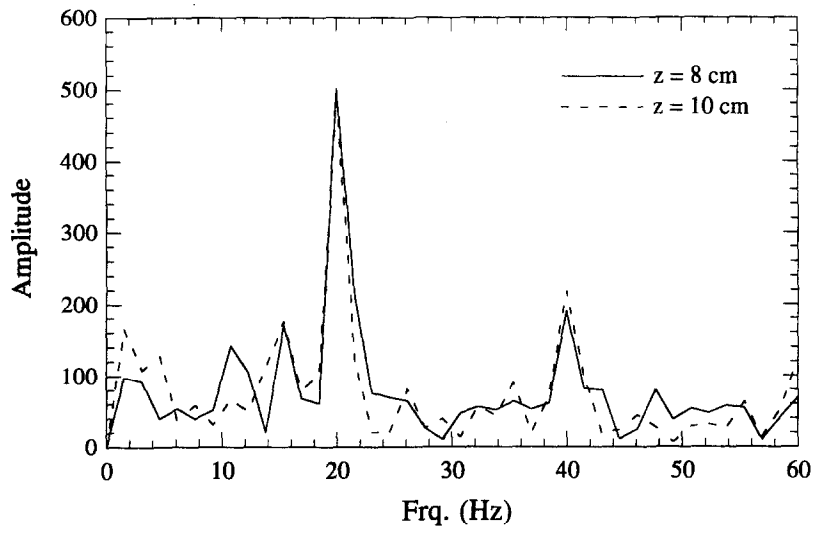

(b)

Fig. 5. Frequency spectra obtained from temperature data recorded within the shear layer at two different axial locations.

values ($M = 0.5$ and 1.0), the structural characteristics seem to change more significantly.

The effect of mass loading in an evaporating spray is depicted in Fig. 8 by plotting the phase-locked instantaneous temperature contours for the three different mass loading values ($M = 0.25$, 0.5 and 1.0). The gas-phase governing equations for this case include all the source/sink terms due to the exchange of mass, momentum and energy due to droplet dynamics and vaporization. Structure of the heated jet seems to change more significantly with the addition of evaporating spray compared to that of a non-evaporating one. Figure 9 shows the time evolution of temperature contours at $z = 7.5$ cm for the three cases shown in Fig. 8. It is interesting to compare the structures of high mass loading values ($M = 0.5$ and 1.0) for the evaporating (Fig. 9) and non-evaporating (Fig. 7) cases. The development of vortical structures for evaporating spray is more periodic than that observed in the corresponding non-evaporating cases. This is probably due to the fact that for the evaporating case the effect of momentum coupling between the phases is reduced due to droplet vaporization.

The effect of dispersed phase on the time-averaged gas-phase properties for both non-evaporating and evaporating sprays with different mass loading values is portrayed in Fig. 10. The time period used in obtaining the average values was at least 10 vortex periods. In addition, it was verified that the average values

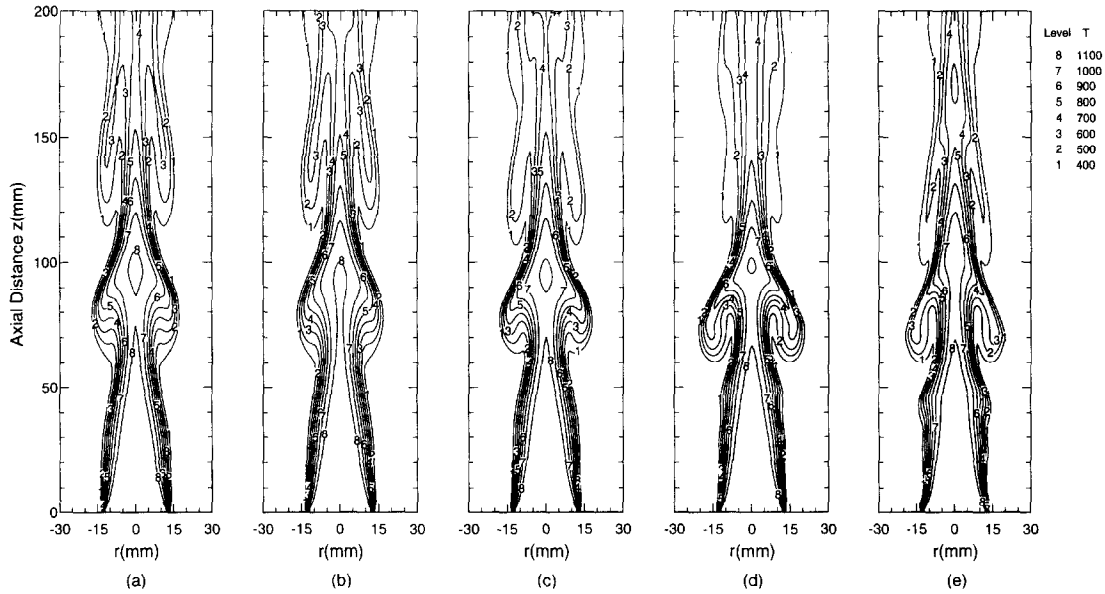

Fig. 6. Instantaneous iso-temperature contours for a 200-μm non-evaporating spray jet with five different mass loading values; (a) $M = 0$, (b) $M = 0.125$, (c) $M = 0.25$, (d) $M = 0.5$ and (e) $M = 1.0$.

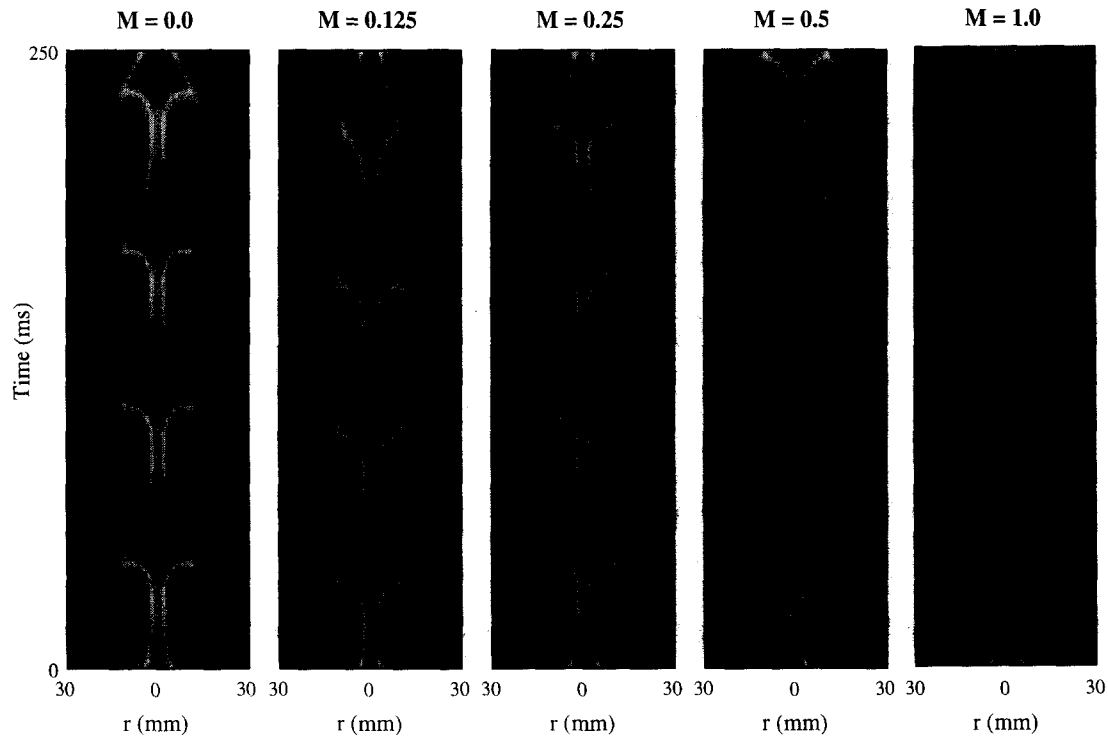

Fig. 7. Time evolution of temperature contours at axial location of 10 cm above inlet for the cases of Fig. 6.

shown in Fig. 10 were independent of this time period. An important observation is that the dispersed phase does not have any discernible influence on the time-averaged properties of non-evaporating spray jet. This is especially interesting in view of the fact that the vortex dynamics for the non-evaporation spray case is modified by the presence of the dispersed phase. As expected, the average gas-phase properties of evaporating spray are significantly affected by the dispersed phase. The average gas temperature decreases along the jet axis due to the cooling caused by droplet vaporization. The decrease in gas temperature reduces the magnitude of buoyant acceleration, resulting in a lowering of average gas velocity compared to that for

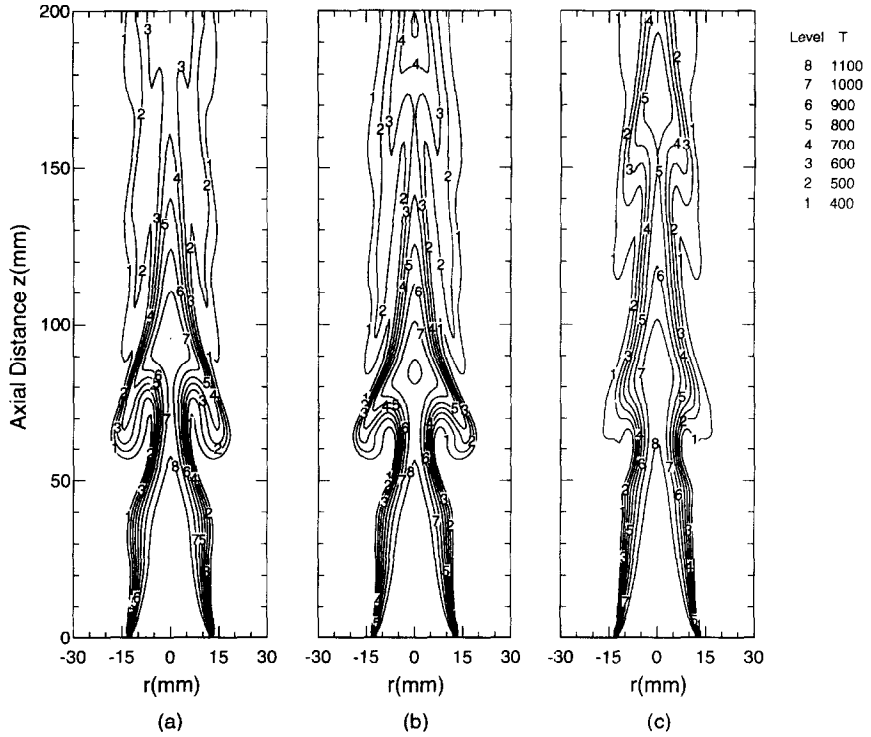

Fig. 8. Instantaneous iso-temperature contours for a 200-μm evaporating spray jet with three different mass loading values; (a) $M = 0.25$, (b) $M = 0.5$ and (c) $M = 1.0$.

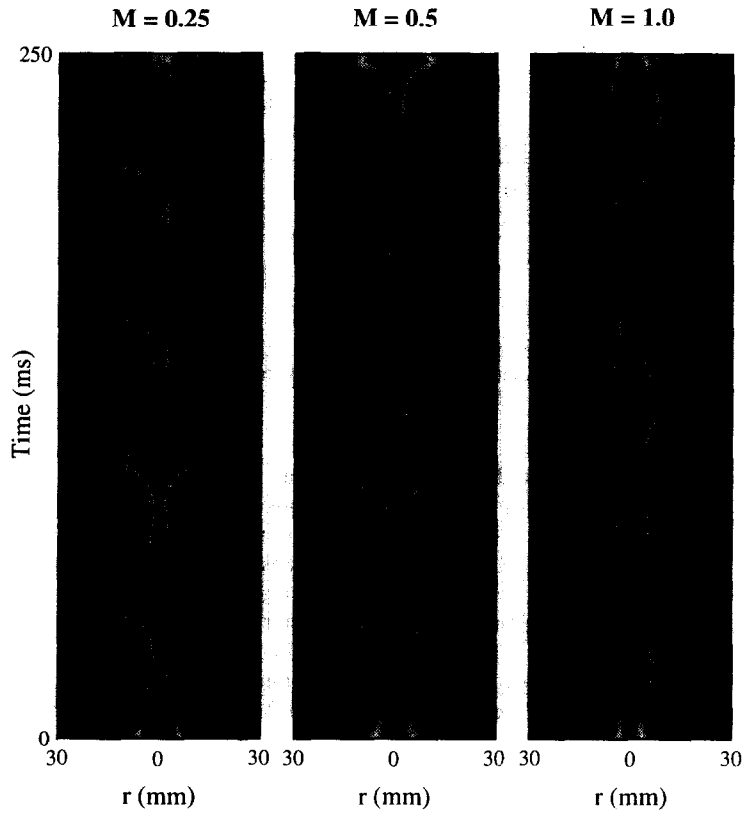

Fig. 9. Time evolution of temperature contours at a location of 7.5 cm above the inlet for the cases of Fig. 8.

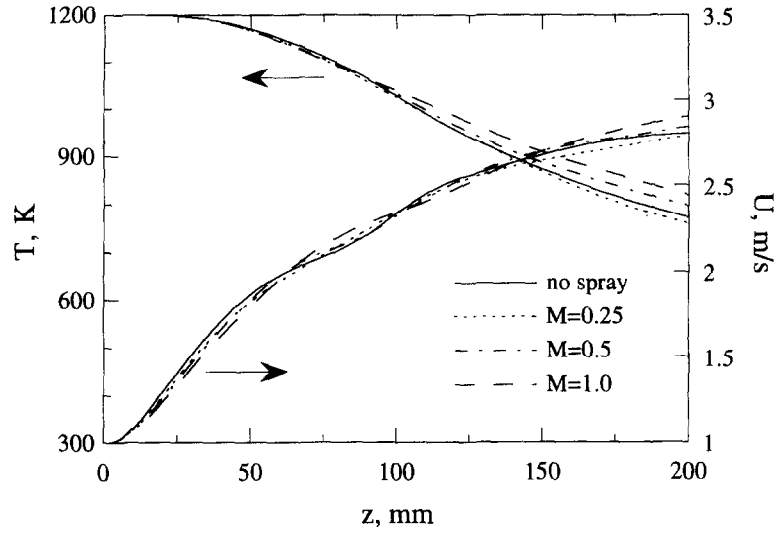

(a)

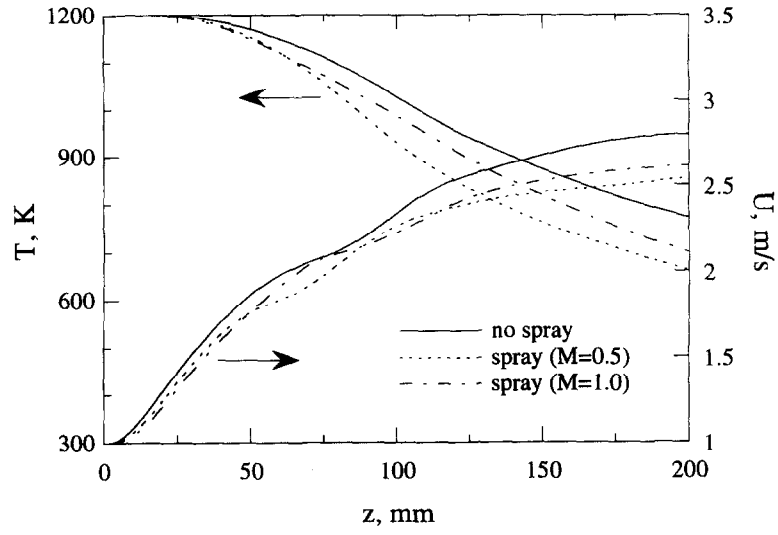

(b)

Fig. 10. Time-averaged axial profiles of gas temperature and axial velocity for (a) non-evaporating and (b) evaporating sprays with different liquid-to-gas loading ratios.

the gaseous case. Note that a reduction in the buoyant acceleration makes the vortex structures weaker as mentioned earlier.

Effect of injection characteristics

The effect of initial droplet distribution on the structural characteristics and dynamics of evaporating spray jet is studied by changing the injection characteristics. The mass loading ratio and droplet diameter are fixed at 1.0 and 200 μm, respectively. The instantaneous temperature contours for three cases having different droplet injection locations are shown in Fig. 11. The three distributions of injection locations used are as follows: (1) $r_k = 1.25$ cm, one injection location, (2) $r_k = 0.625$ and 1.25 cm, two injection locations and (3) $r_k = 0.25$, 0.50, 0.75, 1.00 and 1.25 cm, five injection locations. The mass loading ratio is kept constant by using a different number of droplets in each group for different cases. It is seen that the characteristics of the core region near the nozzle exit are quite different for the three cases due to different droplet injection processes. The use of more injection locations apparently leads to a dynamic heated spray jet with well-organized vortical structures [Fig. 11(c)]. It is known that the vaporization of a liquid droplet absorbs thermal energy and hence reduces the local temperature. This is evident in Figs. 11(b) and (c). In the former figure a valley in the temperature contours

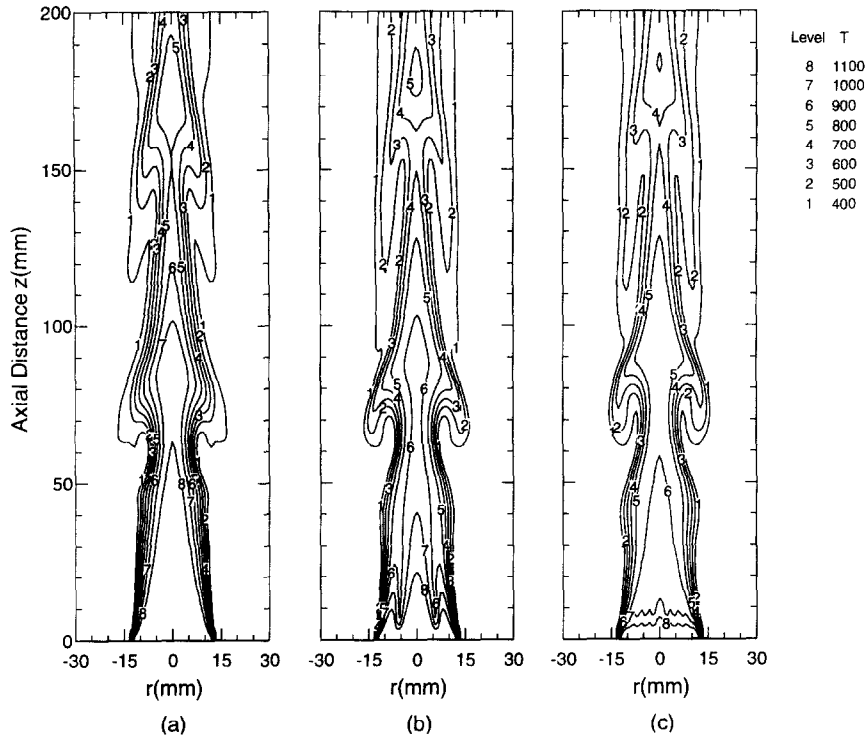

Fig. 11. Instantaneous iso-temperature contours for an evaporating spray jet with three different injection distributions; (a) $r_k = 1.25$ cm, one injection location, (b) $r_k = 0.625$ and 1.25 cm, two injection locations, (c) $r_k = 0.25$, 0.5, 0.75, 1.0 and 1.25 cm, five injection locations.

developed in the downstream region of the inner injection location (i.e. $r_k = 0.625$ cm) as the injected droplet vaporized. However, in the latter figure, the choice of more injection locations reduced the entire jet temperature uniformly leading to near flat contours for 1000 and 1100 K [contours 7 and 8 in Fig. 11(c)]. The time evolution of temperature contours at an axial location of 7.5 cm for the above three cases is plotted in Fig. 12. It clearly shows that the vortex structures are well organized and highly periodic similar to that of a single-phase flow (Fig. 3a) when the number of injection locations is increased. However, the vortex passage frequency for the spray case is different from that for the single-phase jet.

Effect of droplet size

In order to examine the effect of initial droplet size on the processes of droplet-vortex interactions, three different spray cases with initial droplet diameters of 200, 100 and 50 μm are considered. A constant mass loading ratio of $M = 1.0$ is maintained by increasing the number of droplets in each group as its initial size is decreased, and the droplets are injected in the shear layer ($r_k = 1.25$ cm). Results are portrayed in Fig. 13 in the form of snap shots of the flow field. For each case, instantaneous iso-temperature contours and velocity vectors are plotted on the left-hand and right-hand sides of the symmetric jet, respectively. It is quite evident from Fig. 13 that the initial droplet size has a strong influence on the dynamic and structural characteristics of the evaporating spray. For all three cases shown in the figure, there is a reduction in gas temperature due to the vaporization of liquid fuel. However, as the initial droplet size decreases, there is increasingly pronounced cooling in the initial part of the jet caused by droplet vaporization, which affects both the shape and the dynamics of vortex structures. This can be seen more clearly in Fig. 14 which shows the time evolution of vortical structures for the three cases. In fact, when the initial droplet size is sufficiently small ($d_o = 50$ μm), the jet temperature downstream of $z = 6$ cm is reduced to less than 500 K, and vortex structures seem to be destroyed. This drastic reduction in gas temperature is caused by the increased total liquid-phase surface area and entrainment of colder fluid into the jet interior. The latter is due to the vortex merging process and subsequent enlargement of vortex structures for the 50-μm spray case. Note that the vortex merging which occurs at an axial location between $z = 2.5$ and 5 cm is not shown in the figures (although there is some evidence of it in Fig. 13). However, the enlargement of vortex structures for the 50-μm spray can be clearly seen in Fig. 14. The vortex-merging process enhances the entrainment of colder fluid, which further reduces the gas temperature and weakens the vortex structures drastically. Figure 15 shows the effect of initial droplet size on the time-averaged axial profiles of temperature and axial velocity. The drastic reduction in gas temperature caused by droplet vaporization and entrainment of colder fluid, and the subsequent destruction of vortex structures can be clearly seen in this figure. Thus the

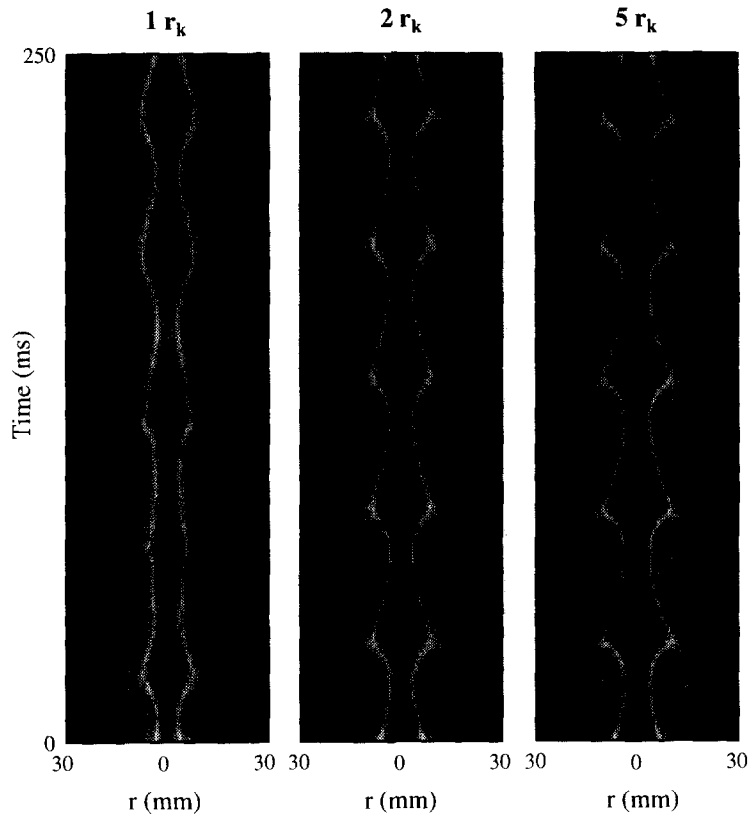

Fig. 12. Time evolution of temperature contours at axial location of 7.5 cm above inlet for the cases of Fig. 10.

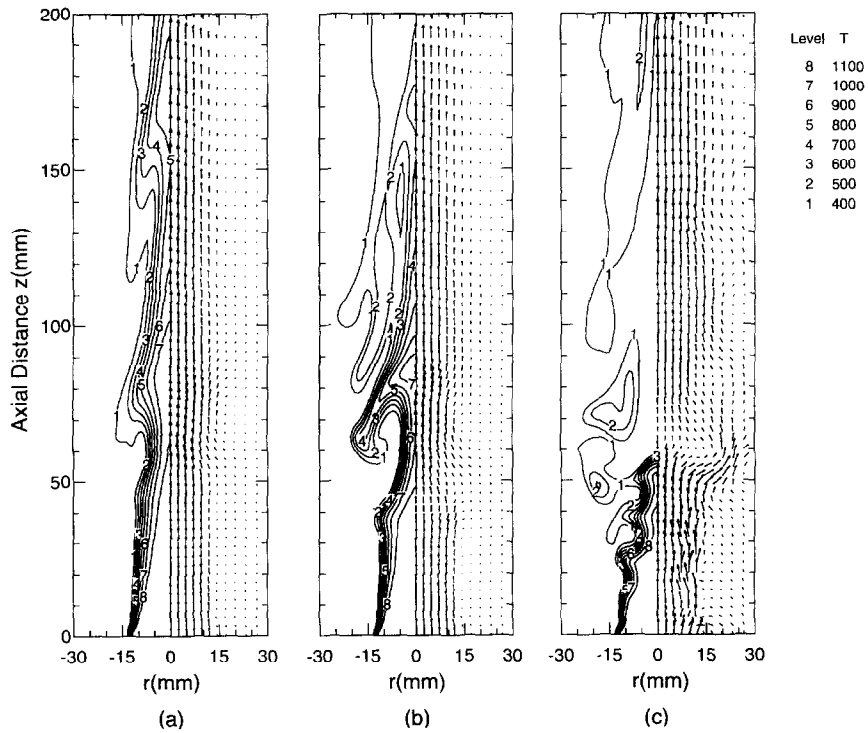

Fig. 13. Simultaneous snapshots of iso-temperature contours and velocity vectors for an evaporating spray for three different initial droplet diameters; (a) $d_o = 200$ μm, (b) $d_o = 100$ μm and (c) $d_o = 50$ μm.

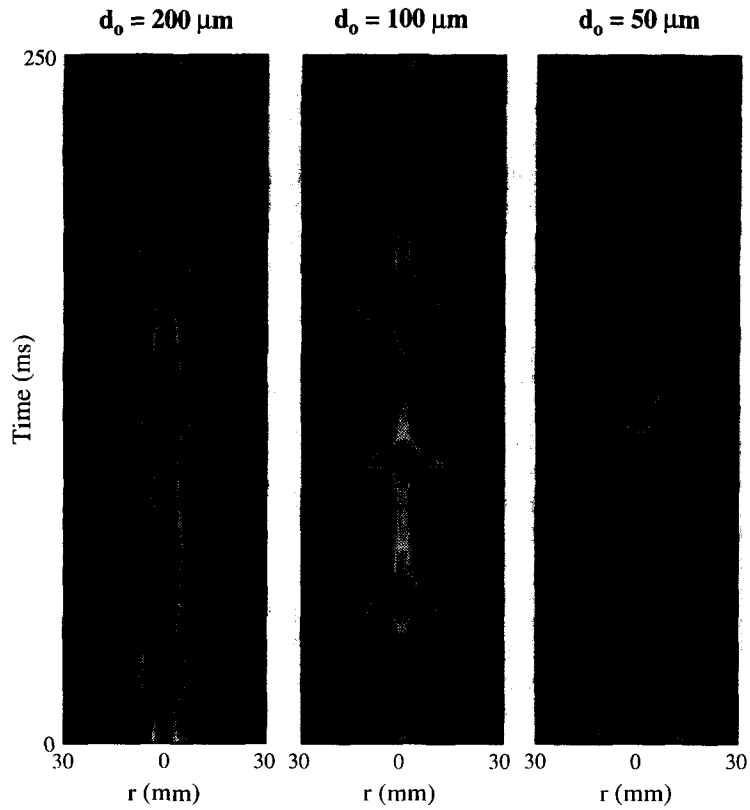

Fig. 14. Time evolution of temperature contours at a location of 7.5 cm above the inlet for the cases of Fig. 12.

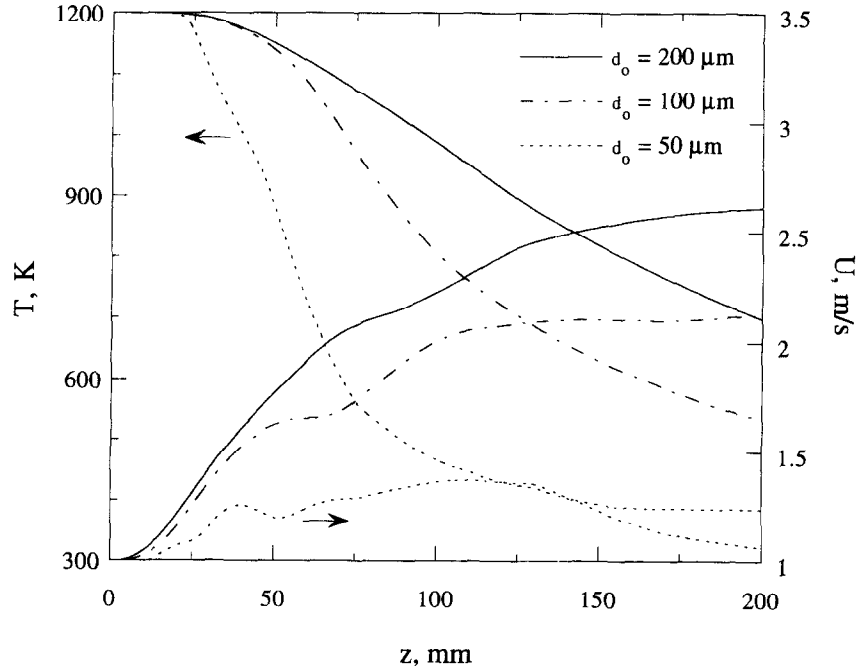

Fig. 15. Time-averaged axial profiles of gas temperature and axial velocity for an evaporating spray with three different initial droplet diameters and $M = 1.0$.

two-way nonlinear interactions seem to become stronger due to fast vaporization of 50-μm spray.

CONCLUSIONS

In this paper, we have investigated the dynamics of two-way droplet-vortex interactions and their influence on the structure of an evaporating spray. A low-speed spray formed (jet Reynolds number based on a jet temperature of 1200 K and velocity of 1.0 m s^{-1} is 154) between a droplet-laden heated nitrogen jet and a coflowing air stream has been simulated. Gravity has been used to generate large-scale vortical structures in the jet shear layer. The density difference between the heated fluid and the cold coflowing fluid gives rise to buoyant acceleration causing vortical structures to appear without any external perturbation. Liquid fuel (n-heptane) droplets are introduced into the vortex structures, and processes of droplet–vortex interactions are studied numerically by developing a time-accurate, multidimensional, two-phase algorithm. The effect of dispersed phase is incorporated through the source/sink terms in the gas-phase governing equations, representing the exchange of mass, momentum, and energy between the gas and liquid phases.

Snapshots and time evolution plots of vortex structures have been employed to analyze the effect of dispersed phase on their dynamics and time-averaged behavior under different mass loadings for both non-evaporating and evaporating sprays. The vortex structures cause droplets to disperse radially outward, and this in turn determines the fuel vapor distribution and also modifies the vortex dynamics. Thus, the dynamics and structural characteristics of the evaporating spray are strongly influenced by these interactions. The effects of initial droplet size, injection location, and liquid-to-gas mass loading ratio on the droplet–vortex interaction have been investigated by performing numerical experiments.

For both non-evaporating and evaporating sprays, the effect of dispersed phase on vortex dynamics is found to be negligible for mass loading ratio (M) less than 0.5. However, at higher loading ratios, depending upon the droplet injection characteristics, the vortex dynamics as well as the spray jet behavior may be strongly influenced by the dispersed phase. For a non-evaporating spray, the dispersed phase modifies the dynamics of vortex structures but not the time-average behavior, while it modifies both the dynamics and time-averaged behavior for an evaporating spray. For example, for 200-μm spray at $M = 1.0$ and with droplets injected into the shear layer, the vortex passage frequency is increased by about 30% and the vortex structures become weaker and less coherent compared to the gaseous jet case. This has important implications in spray applications such as gas turbine and ramjet combustors, especially when the system performance is strongly linked to some underlying unsteady phenomenon. Results also indicate that the initial droplet size has a strong influence on the two-way interactions. Due to spray vaporization, gas temperature in the jet interior decreases, which modifies the vortex dynamics and consequently the droplet dynamics and vaporization. In fact, for 50-μm spray at $M = 1.0$, the vortex dynamics is drastically modified and a vortex pairing phenomenon is observed. The latter results in a much larger entrainment of colder fluid causing a subsequent destruction of vortex structures. Thus the spray injection characteristics have strong influence on the processes of droplet–vortex interactions.

Acknowledgements—This work was funded by the AFOSR under Grant F49620-93-1-0400 monitored by Dr Julian M. Tishkoff. Many fruitful discussions with Dr W. M. Roquemore at Wright-Patterson Air Force Base are greatly appreciated. Computations were performed on Cray C-90 at the Pittsburgh Supercomputing Center.

REFERENCES

1. G. L. Brown and A. Roshko, Density effects and large scales in the developing mixing layer, *J. Fluid Mech.* **64,** 775–816 (1974).
2. A. J. Yule, Large scale structure in the mixing layer of a round jet, *J. Fluid Mech.* **89,** 413–432 (1978).
3. V. R. Katta, L. P. Goss and W. M. Roquemore, Effect of nonunity Lewis number and finite-rate chemistry on the dynamics of a hydrogen–air jet diffusion flame, *Combust. Flame* **96,** 60–74 (1994).
4. E. K. Longmire and J. K. Eaton, Structure of a particle-laden round jet, *J. Fluid Mech.* **236,** 217–257 (1992).
5. J. N. Chung and T. R. Troutt, Simulation of particle dispersion in an axisymmetric jet, *J. Fluid Mech.* **186,** 199–222 (1988).
6. D. Hansell, I. M. Kennedy and W. Kollmann, A simulation of particle dispersion in a turbulent jet, *Int. J. Multiphase Flow* **18,** 559–576 (1992).
7. B. J. Lazaro and J. C. Lasheras, Particle dispersion in the developing free shear layer—I. Unforced flow, *J. Fluid Mech.* **235,** 143–178 (1992).
8. B. J. Lazaro and J. C. Lasheras, Particle dispersion in the developing free shear layer—II. Forced flow, *J. Fluid Mech.* **235,** 179–221 (1992).
9. M. Samimy and S. K. Lele, Motion of particles with inertia in a compressible free layer, *Phys. Fluids* **A3,** 1915–1923 (1991).
10. K. Hishida, A. Ando and M. Maeda, Experiments on particle dispersion in a turbulent mixing layer, *Int. J. Multiphase Flow* **18,** 181–194 (1992).
11. J. Uthuppan, S. K. Aggarwal, F. F. Grinstein and K. Kailasanath, Particle dispersion in a transitional axisymmetric jet: a numerical simulation, *AIAA J.* **32,** 2004–2014 (1994).
12. S. K. Aggarwal, Relationship between stokes number and intrinsic frequencies in particle laden flows, *AIAA J.* **32,** 1322–1325 (1994).
13. T. W. Park, S. K. Aggarwal and V. R. Katta, Gravity effects on the dynamics of evaporating droplets in a heated jet, *AIAA J. Propulsion Power* **11,** 519–528 (1995).
14. B. Abramzon and W. A. Sirignano, Droplet vaporization model for spray combustion calculations, *Int. J. Heat Mass Transfer* **32,** 1605–1618 (1989).
15. D. K. Edwards, V. E. Denny and A. F. Mills, *Transfer Processes: An Introduction to Diffusion, Convection and Radiation* (2nd Edn). McGraw-Hill, New York (1979).
16. S. K. Aggarwal, A. Tong and W. A. Sirignano, A comparison of vaporization models for spray calculation, *AIAA J.* **22,** 1448–1457 (1984).
17. B. P. Leonard, A stable and accurate convective mod-

elling procedure based on quadratic upstream interpolation, *Comput. Meth. Appl. Mech. Engng* **19,** 59–98 (1979).
18. D. B. Spalding, A novel finite difference formulation for difference expressions involving both first and second derivatives, *Int. J. Numer. Meth. Engng* **4,** 551–559 (1972).
19. P. A. Monkewitz and K. D. Sohn, Absolute instability in hot jets, *AIAA J.* **26,** (8), 911–916 (1988).
20. S. Ragu and P. A. Monkewitz, The bifurcation of a hot round jet to limit-cycle oscillations, *Phys. Fluids A* **3,** 501–503 (1991).
21. L.-D. Chen, J. P. Seaba, W. M. Roquemore and L. P. Gross, Buoyant diffusion flames, *Proceedings Twenty-Second International Symposium on Combustion*, pp. 677–684. The Combustion Institute, Pittsburgh, PA (1988).
22. H. Eickhoff and A. Winandy, Visualization of vortex formation in jet diffusion flames, *Combust. Flame* **60** (1), 99–101 (1985).
23. T. Yuan, D. Durox and E. Villermaux, An analog study for flame flickering, *Expts Fluids* **17** (5), 337–349 (1994).
24. R. W. Davis, E. F. Moore, W. M. Roquemore, L.-D. Chen, V. Vilimpoc and L. P. Goss, Preliminary results of a numerical–experimental study of the dynamic structure of a buoyant jet diffusion flame, *Combust. Flame* **83** (3/4), 263–270 (1991).
25. V. R. Katta, L. P. Goss and W. M. Roquemore, Numerical investigations of transitional H_2/N_2 jet diffusion flames, *AIAA J.* **32,** 84–94 (1994).